

Omnidirectional Radiation in the Presence of Homogenized Metasurfaces

David Di Ruscio^{1, *}, Paolo Burghignoli², Paolo Baccarelli², and Alessandro Galli²

Abstract—Analytical and numerical approaches are presented for modeling the interaction of azimuthally symmetric fields with omnidirectional metasurfaces, based on the use of locally homogenized equivalent sheet impedances. Radially uniform metasurfaces on layered dielectric media are described in terms of a spectral impedance dyadic, thus allowing for the derivation of the field excited by omnidirectional sources through a simple transmission-line model. In a first approximation, the effect of circular edges in laterally truncated structures is taken into account through an efficient physical-optics method. Then, truncated and radially non-uniform homogenized layered structures are treated numerically with the method of moments, by suitably extending a recently developed spectral-domain formulation. Numerical results are presented for planar radiating structures based on omnidirectional metasurfaces, comparing the radiation patterns obtained through the proposed homogenized models with those calculated by means of full-wave simulations. The discussion emphasizes the validity of the proposed approaches and their usefulness in the analysis of two-dimensional leaky-wave antennas based on printed omnidirectional metasurfaces.

1. INTRODUCTION AND BACKGROUND

Azimuthally symmetric planar structures have recently been considered for the realization of, e.g., printed antennas [1–8], enhanced electromagnetic-wave transmission through a subwavelength aperture [9, 10], plasmonic lenses [11–14], and optoelectronic applications [15–18]. In particular, the possibility of producing azimuthally symmetric fields has attracted interest for antenna designs with conical radiation patterns and reconfigurable polarization [19], which may be employed in Local Area Networks [20–23] as well as in radio links between satellites and moving vehicles [24–26]. In this framework, two-dimensional (2-D) leaky-wave antennas (LWAs) provide versatile, low-profile, and low-cost solutions for achieving directive radiation patterns, in the form of conical scanned or broadside pencil beams [27]. Typical examples are Fabry-Pérot cavity antennas in which a simple source excites a parallel-plate waveguide whose upper plate is a partially-reflecting surface (PRS) [28–31]. The PRS may be a uniform dielectric medium or a periodic screen, e.g., a printed metasurface, which can be represented, in the low-frequency regime, as an equivalent uniform homogenized surface [32–34].

When a narrow-beam 2-D LWA is designed, the attenuation constant of the leaky mode responsible of radiation is small, and hence the leaky mode extends to appreciable distances from the source, in terms of free-space wavelengths, before being sufficiently attenuated to achieve typical radiation efficiencies (e.g., 90%) [27]. Calculating the radiation pattern for such large structures requires challenging numerical simulations with commercial electromagnetic (EM) software and is a time consuming process. Hence, there is the need for approximate analytical and ad hoc full-wave numerical methods for the fast analysis and design of such a kind of LWAs.

Received 15 December 2014, Accepted 5 February 2015, Scheduled 16 February 2015

* Corresponding author: David Di Ruscio (d.diruscio@idscorporation.com).

¹ IDS Corporation, Via E. Calabresi 24, Pisa 56121, Italy. ² Department of Information Engineering, Electronics and Telecommunications, Sapienza University of Rome, Rome 00184, Italy.

In this work we study a class of structures constituted by an omnidirectional metasurface embedded in a multilayered environment (in what follows we will use, for the sake of brevity, the term metasurface to indicate any textured surface that can be analytically treated under the homogenization theory [35–38]). In particular, we consider thin texture metal screens characterized by the following properties: *i*) at any point (ρ, ϕ) (in cylindrical coordinates) the screen texture can be *linearized* resulting in a periodic geometry (i.e., the screen is locally periodic) as shown in Fig. 1; *ii*) the locally linearized screen can be described in terms of a suitable surface impedance dyadic $\underline{\mathbf{Z}}_S^{lin}$ through the following transition conditions:

$$\tilde{\mathbf{E}}_t^+(\mathbf{k}'_t) = \tilde{\mathbf{E}}_t^-(\mathbf{k}'_t) \left(= \tilde{\mathbf{E}}_t(\mathbf{k}'_t) \right) \quad (1)$$

$$\tilde{\mathbf{E}}_t(\mathbf{k}'_t) = \underline{\mathbf{Z}}_S^{lin}(\mathbf{k}'_t; \rho, \phi) \cdot \tilde{\mathbf{J}}_S(\mathbf{k}'_t) = \underline{\mathbf{Z}}_S^{lin}(\mathbf{k}'_t; \rho, \phi) \cdot \mathbf{z}_0 \times \left[\tilde{\mathbf{H}}_t^+(\mathbf{k}'_t) - \tilde{\mathbf{H}}_t^-(\mathbf{k}'_t) \right] \quad (2)$$

where the subscript ‘*t*’ stands for ‘tangential’; the tilde indicates a spectral-domain quantity; $\mathbf{k}'_t = k'_x \mathbf{x}_0 + k'_y \mathbf{y}_0$ is the (local) wavevector; the superscripts $+/-$ indicate the upper/lower faces of the textured screen, respectively; *iii*) the surface impedance dyadic $\underline{\mathbf{Z}}_S^{lin}$ is assumed to be independent of the azimuthal coordinate ϕ : $\underline{\mathbf{Z}}_S^{lin} = \underline{\mathbf{Z}}_S^{lin}(\mathbf{k}'_t; \rho)$ (i.e., the metasurface is *omnidirectional*).

A typical case of interest for antenna applications, that will be assumed in the following as a reference structure, is that of a grounded dielectric multilayer covered with an electrically thin metal screen with annular geometry (an *annular* metasurface), as shown in Fig. 1. A simple example of printed annular metasurface is a radial array of concentric annular slots or strips. Radial arrays of annularly disposed printed cells, such as rectangular patches or Jerusalem cross structures, belong to this class of metasurfaces as well.

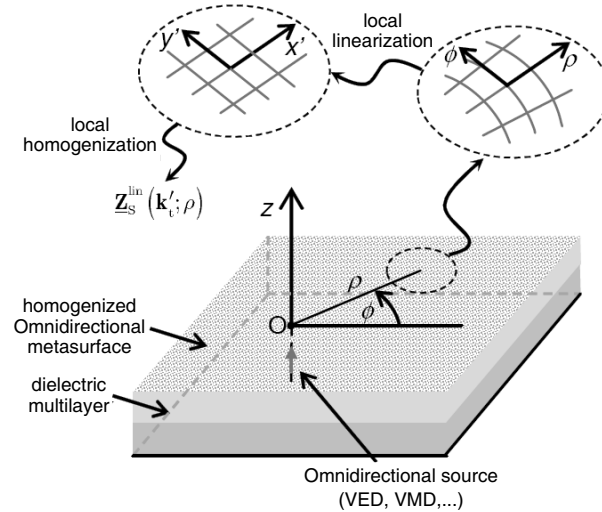


Figure 1. Reference structure and relevant coordinate system: a grounded dielectric multilayer covered with an annular metasurface. The latter is represented through a locally homogenized surface impedance dyadic independent of the azimuthal coordinate (*omnidirectional homogenized metasurface*).

The structure is assumed to be excited by an omnidirectional source, such as a vertical electric dipole (VED), a vertical magnetic dipole (VMD), a horizontal electric ring, etc.. Since the geometry is omnidirectional as well, the excited field will be azimuthally symmetric. The aim of this work is to provide analytical and numerical tools for an accurate and rapid determination of such a field, with particular reference to the radiation pattern in the far-field region.

Radially uniform omnidirectional metasurfaces will be considered first (Sections 2.1 and 2.2), for which the local surface impedance is independent of the radial coordinate $\underline{\mathbf{Z}}_S^{lin} = \underline{\mathbf{Z}}_S^{lin}(\mathbf{k}'_t)$. A transmission-line based equivalent model is derived for this case, based on the use of $\underline{\mathbf{Z}}_S^{lin}$, which allows for calculating analytically the far field radiated by a VED or VMD. Edge effects in laterally

truncated structures are also taken into account, by adopting a suitable numerically efficient physical-optics approach (Section 2.3). This may find application to, e.g., the design of Fabry-Pérot cavity antennas with broadside pencil or conical scanned beams.

A numerical approach is then developed (Section 2.4), by suitably extending a recently derived spectral formulation of the method of moments (MoM) tailored to the treatment of azimuthally symmetric problems [39]. By means of this numerical method, truncated structure are accurately studied and the results of the PO approach are validated and further refined. However, the MoM formulation is valid only for LWAs based on omnidirectional metasurface which are not spatially dispersive or where a *dominant* leaky wave fully characterizes the aperture field. Radially non-uniform metasurfaces can be also considered by the MoM approach, whereas the radial dependence of the local surface impedance prevents from establishing a simple network model. The class of structures that can be studied is thus enlarged, including, e.g., 2-D LWAs with a radially tapered illumination function [40].

Numerical results are presented and discussed (Section 3) on specific examples of metasurface-based planar radiators, comparing the proposed analytical and numerical formulations with rigorous full-wave simulations, either obtained with in-house MoM codes or with FEKO [41], a general-purpose commercial electromagnetic (EM) simulator based on the MoM in the space domain and using Rao-Wilton-Glisson basis functions [42].

2. ANALYTICAL AND FULL-WAVE NUMERICAL APPROACHES FOR OMNIDIRECTIONAL HOMOGENIZED STRUCTURES

In this section we will develop suitable equivalent-network models for the analysis of omnidirectional metasurfaces with a locally homogenized surface impedance *independent* of the *radial* coordinate ρ and function of the spectral wavenumber \mathbf{k}'_t (which accounts for the *non-local* nature of the surface impedance), i.e., $\underline{\mathbf{Z}}_S^{lin} = \underline{\mathbf{Z}}_S^{lin}(\mathbf{k}'_t)$. Truncation effects will be considered approximately with a physical-optics (PO) approach. Furthermore, a tailored full-wave numerical method will be presented for the rigorous analysis of truncated structures, which can also consider a class of radially non-uniform metasurfaces.

2.1. Omnidirectional Homogenized Equivalent-Network Model

As is well known, the enforcing, in the Fourier spectral domain, of an impedance boundary condition as (2), which is valid for thin screen and describes the relation between the tangential component of the average electric field $\tilde{\mathbf{E}}_t(\mathbf{k}_t)$ and the average surface electric current $\tilde{\mathbf{J}}_S(\mathbf{k}_t)$, requires a translationally invariant structure. In this case, in fact, the aforementioned constitutive relation corresponds to a convolutional product in the spatial domain. Unfortunately, the class of structures analyzed in this paper is not translational invariant, thus preventing, strictly speaking, to establish an impedance boundary condition.

The spectral and the spatial representations of omnidirectional fields and currents, which depend only on the distance from the origin, i.e., $\rho = \sqrt{x^2 + y^2}$, are related to each other by means of a Fourier-Bessel transform of the first order (\mathcal{FB}_1), that is

$$\begin{aligned}\tilde{\mathbf{E}}_t(k_\rho) &= 2\pi j \int_0^\infty \rho E_\rho(\rho) J_1(k_\rho \rho) d\rho \mathbf{u}_0 + 2\pi j \int_0^\infty \rho E_\phi(\rho) J_1(k_\rho \rho) d\rho \mathbf{v}_0 \\ &= 2\pi j \mathcal{FB}_1 \{E_\rho\} \mathbf{u}_0 + 2\pi j \mathcal{FB}_1 \{E_\phi\} \mathbf{v}_0 = \tilde{E}_u(k_\rho) \mathbf{u}_0 + \tilde{E}_v(k_\rho) \mathbf{v}_0\end{aligned}\quad (3)$$

$$\begin{aligned}\tilde{\mathbf{J}}_t(k_\rho) &= 2\pi j \int_0^\infty \rho J_\rho(\rho) J_1(k_\rho \rho) d\rho \mathbf{u}_0 + 2\pi j \int_0^\infty \rho J_\phi(\rho) J_1(k_\rho \rho) d\rho \mathbf{v}_0 \\ &= 2\pi j \mathcal{FB}_1 \{J_\rho\} \mathbf{u}_0 + 2\pi j \mathcal{FB}_1 \{J_\phi\} \mathbf{v}_0 = \tilde{J}_u(k_\rho) \mathbf{u}_0 + \tilde{J}_v(k_\rho) \mathbf{v}_0\end{aligned}\quad (4)$$

where $\mathbf{u}_0 = \mathbf{k}_t/|\mathbf{k}_t|$ and $\mathbf{v}_0 = \mathbf{z}_0 \times \mathbf{u}_0$ are the unit vectors that define the TM/TE basis, J_1 is the Bessel function of first kind of order 1, and $k_\rho = |\mathbf{k}_t|$. Being inspired by this simplicity and assuming that what follows holds only for symmetric fields interacting with omnidirectional metasurfaces independent of the radial coordinate ρ , an impedance boundary condition of the kind (2) is imposed directly in the

Fourier-Bessel spectral domain, thus having

$$\tilde{\mathbf{E}}_t(k_\rho) = \underline{\mathbf{Z}}_S(k_\rho) \cdot \tilde{\mathbf{J}}_S(k_\rho) \quad (5)$$

where

$$\underline{\mathbf{Z}}_S(k_\rho) = Z_S^{\text{TM}}(k_\rho) \mathbf{u}_0 \mathbf{u}_0 + Z_S^{\text{TM/TE}}(k_\rho) \mathbf{u}_0 \mathbf{v}_0 + Z_S^{\text{TE/TM}}(k_\rho) \mathbf{v}_0 \mathbf{u}_0 + Z_S^{\text{TE}}(k_\rho) \mathbf{v}_0 \mathbf{v}_0 \quad (6)$$

When the metasurface does not introduce any cross-coupling between the two polarizations, i.e., $Z_S^{\text{TE/TM}}(k_\rho) = Z_S^{\text{TM/TE}}(k_\rho) = 0$, the boundary condition (5) simplifies. Considering for example the TM case we have

$$\tilde{E}_u(k_\rho) = Z_S^{\text{TM}}(k_\rho) \tilde{J}_u(k_\rho) \quad (7)$$

or equivalently, introducing the admittance $Y_S^{\text{TM}}(k_\rho) = 1/Z_S^{\text{TM}}(k_\rho)$,

$$\tilde{J}_u(k_\rho) = Y_S^{\text{TM}}(k_\rho) \tilde{E}_u(k_\rho) \quad (8)$$

It is worth noting that a method for the direct calculation of $\underline{\mathbf{Z}}_S(k_\rho)$ is needed for Equation (5) to be useful. To this aim, the hypothesis that the omnidirectional field, in terms of an omnidirectional cylindrical wave, locally interacts with the annular metasurface as the corresponding plane wave interacts with the linearized structure is assumed. Let then $\underline{\mathbf{Z}}_S^{\text{lin}} = \underline{\mathbf{Z}}_S^{\text{lin}}(k'_x, k'_y)$ be the spectral surface impedance dyadic of the locally linearized structure, referred to local Cartesian axes (x', y') (see Fig. 1). Since an omnidirectional cylindrical wave with radial wavenumber k_ρ locally travels along ρ (i.e., x'), its interaction with the metasurface can be described in terms of $\underline{\mathbf{Z}}_S^{\text{lin}}(k'_x = k_\rho, k'_y = 0)$ and the components of the dyadic impedance are

$$\begin{aligned} Z_S^{\text{TM}}(k_\rho) &= Z_{S,x'x'}^{\text{lin}}(k_\rho, 0) \\ Z_S^{\text{TM/TE}}(k_\rho) &= Z_{S,x'y'}^{\text{lin}}(k_\rho, 0) \\ Z_S^{\text{TE/TM}}(k_\rho) &= Z_{S,y'x'}^{\text{lin}}(k_\rho, 0) \\ Z_S^{\text{TE}}(k_\rho) &= Z_{S,y'y'}^{\text{lin}}(k_\rho, 0) \end{aligned} \quad (9)$$

In conclusion, whereas (5) has the customary form of an impedance boundary condition valid for thin screens, its use in the present context is *unconventional* since the metasurface is *not* translationally invariant. However, (5) is assumed here to be used only for describing the interaction of the metasurface with omnidirectional cylindrical waves, such as those produced by an azimuthally symmetric source. We finally note that the form of (6), whose coefficients in the TM/TE bases are functions of $k_\rho = |\mathbf{k}_t|$ only, exactly reflects the assumed rotational invariance of the homogenized metasurface. Furthermore, the non-local nature of the surface impedance dyadic is fully taken into account by its dependence with k_ρ , in contrast to different approaches where the spatial dispersion is considered approximately by evaluating the impedance at a specific average wavenumber [34].

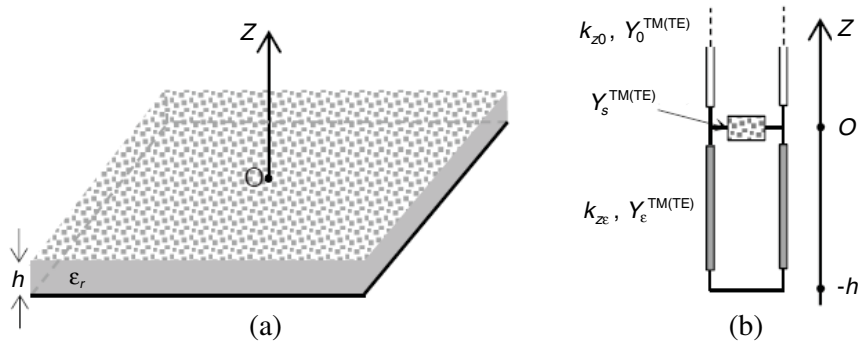


Figure 2. (a) Grounded dielectric slab covered with a homogenized omnidirectional metasurface modeled through (5), (6). (b) Relevant transverse equivalent network (TEN).

Let us now consider an omnidirectional (i.e., ϕ -independent) cylindrical wave with radial wavenumber k_ρ propagating along the considered structure. A transmission-line model along z can be easily established in any homogeneous region of the dielectric multilayer in which the metasurface is embedded (see Fig. 2). As a consequence of (5), and assuming that no TM/TE coupling occurs (i.e., $Z_S^{\text{TM/TE}} = Z_S^{\text{TE/TM}} = 0$), the structure can be modeled through a transverse equivalent network (TEN) in which the metasurface is represented by a simple shunt admittance Y_S^{TM} or Y_S^{TE} for TM or TE fields, respectively [43]. For the TM polarization we assume transverse fields in a factorized form: $E_\rho(\rho, z) = e_\rho(\rho)V^{\text{TM}}(z)$, $H_\phi(\rho, z) = h_\phi(\rho)I^{\text{TM}}(z)$, where e_ρ, h_ϕ are modal functions and $V^{\text{TM}}, I^{\text{TM}}$ are the equivalent modal voltage and current, respectively. For the TE polarization we assume, dually, $E_\phi(\rho, z) = e_\phi(\rho)V^{\text{TE}}(z)$, $H_\rho(\rho, z) = -h_\rho(\rho)I^{\text{TE}}(z)$, where e_ϕ, h_ρ are modal functions and $V^{\text{TE}}, I^{\text{TE}}$ are the equivalent modal voltage and current, respectively. The TEN can then be used for, e.g., the determination of the modal wavenumber k_ρ of surface and leaky modes supported by the structure, or the calculation of the field produced by elementary omnidirectional sources; the latter is illustrated in the next subsection.

2.2. Far-field Pattern for Infinite Structures

The far field produced by a VED (or a VMD) placed on the z axis at $z = z_0$ in the presence of a *laterally infinite* structure can be calculated using reciprocity theorem, considering an appropriate test source. Typically, an electric or magnetic point dipole is chosen as a test source in the far field [28], producing a plane wave that interacts with the stratified medium. However, for (5) and (6) to be valid, the test source should give rise to an incident field in the form of an omnidirectional cylindrical wave. Hence, a magnetic (or electric) ring has been chosen as a test source in the far region and the field at the source location has been determined using the relevant TEN (details of the calculation are reported in Appendix A).

Considering for instance a VED source with amplitude $P_0 [A \cdot m]$, this excites a TM field with far-field components E_θ, H_ϕ given by

$$H_\phi(r, \theta) = \frac{1}{\eta_0} E_\theta(r, \theta) = \frac{P_0}{\varepsilon_r} j k_0 \sin \theta C(\theta) \frac{e^{-jk_0 r}}{4\pi r} \quad (10)$$

Here ε_r is the relative permittivity at the source location whereas $C(\theta)$ is a constant that depends on the specific stratified medium (it is the ratio between the current at $z = z_0$ and the incident current at $z = 0$ in the relevant TEN). If the structure is constituted by a single grounded dielectric layer with thickness h (see Fig. 2), it results in

$$C(\theta) = -\frac{Y_{in}^{\text{TM}}}{Y_{in}^{\text{TM}} + Y_S^{\text{TM}}} \frac{Y_{in}^{\text{TM}} - Y_0^{\text{TM}} \cos[k_{z\varepsilon}(z_0 + h)]}{Y_{in}^{\text{TM}} + Y_0^{\text{TM}} \cos(k_{z\varepsilon}h)} \quad (11)$$

where $Y_{in}^{\text{TM}} = -jY_\varepsilon^{\text{TM}} \cot(k_{z\varepsilon}h)$, $Y_S^{\text{TM}} = 1/Z_S^{\text{TM}}$, and the TEN parameters for the TM polarization are

$$\begin{aligned} Y_0^{\text{TM}} &= \frac{k_0}{\eta_0 k_{z0}} & k_{z0} &= k_0 \cos \theta \\ Y_\varepsilon^{\text{TM}} &= \frac{k_0 \varepsilon_r}{\eta_0 k_{z\varepsilon}} & k_{z\varepsilon} &= k_0 \sqrt{\varepsilon_r - \sin^2 \theta} \end{aligned} \quad (12)$$

Considering now a VMD source with amplitude $Q_0 [V \cdot m]$, this excites a TE field with far-field components E_ϕ, H_θ ; these can be obtained from (10) by duality:

$$E_\phi(r, \theta) = \eta_0 H_\theta(r, \theta) = -\frac{Q_0}{\mu_r} j k_0 \sin \theta C'(\theta) \frac{e^{-jk_0 r}}{4\pi r} \quad (13)$$

Here μ_r is the relative permittivity at the source location whereas $C'(\theta)$ is a constant that depends on the specific stratified medium (it is the ratio between the voltage at $z = z_0$ and the incident voltage at $z = 0$ in the relevant TEN). If the structure is constituted by a single grounded dielectric layer with thickness h and $\mu_r = 1$, it results in

$$C'(\theta) = \frac{Y_0^{\text{TE}}}{Y_0^{\text{TE}} + Y_{in}^{\text{TE}} + Y_S^{\text{TE}}} \frac{\sin[k_{z\varepsilon}(z_0 + h)]}{\sin(k_{z\varepsilon}h)} \quad (14)$$

where $Y_{in}^{\text{TE}} = -jY_{\varepsilon}^{\text{TE}} \cot(k_{z\varepsilon}h)$, $Y_S^{\text{TE}} = 1/Z_S^{\text{TE}}$, and the TEN parameters for the TE polarization are

$$\begin{aligned} Y_0^{\text{TE}} &= \frac{k_{z0}}{k_0\eta_0} & k_{z0} &= k_0 \cos \theta \\ Y_{\varepsilon}^{\text{TE}} &= \frac{k_{z\varepsilon}}{k_0\eta_0} & k_{z\varepsilon} &= k_0 \sqrt{\varepsilon_r - \sin^2 \theta} \end{aligned} \quad (15)$$

2.3. Far-Field Pattern for Truncated Structures

The far field produced by a VED (or a VMD) placed on the z axis at $z = z_0$ in the presence of a *truncated* structure can be calculated approximately by resorting to the PO approach developed in [44]. The approximation made in [44] is that the circular aperture is terminated at some arbitrary radius by a perfect absorber, hence reflected waves and fringe deformations of the currents at the circular truncations are neglected.

According to [44], the far-field pattern is expressed by a single spectral integral in k_{ρ} involving the product of the spectral aperture field at $z = 0$ and a suitable weighting function. In particular, for the the TM case the pattern is

$$P_{\theta}(\theta) = -\frac{\eta_0}{k_0\varepsilon_r} \int_0^{+\infty} k_{\rho}^2 V_v^{\text{TM}}(k_{\rho}) P_0(k_{\rho}, \theta) dk_{\rho} \quad (16)$$

whereas in the TE case

$$P_{\theta}(\theta) = \int_0^{+\infty} k_{\rho}^2 V_i^{\text{TE}}(k_{\rho}) P_0(k_{\rho}, \theta) dk_{\rho} \quad (17)$$

Here the functions V_v^{TM} , V_i^{TE} are the TEN voltages at $z = 0$ due to a unit-amplitude voltage or current generator, respectively, placed at the source location. The weighting function $P_0(k_{\rho}, \theta)$, presented in [44] for a circular aperture, is reported here, for the sake of completeness, in the more general case of an annular aperture with inner radius a and outer radius b ; this allows for modeling truncated metasurfaces with a central circular metal region of radius a . For both TM and TE polarizations, $P_0(k_{\rho}, \theta)$ is given by

$$P_0(k_{\rho}, \theta) = \frac{1}{k_{\rho}^2 - \xi^2} [\xi b J_1(k_{\rho}b) J_0(\xi b) - \xi a J_1(k_{\rho}a) J_0(\xi a) - k_{\rho} b J_1(\xi b) J_0(k_{\rho}b) + k_{\rho} a J_1(\xi a) J_0(k_{\rho}a)] \quad (18)$$

where $\xi = k_0 \sin \theta$.

2.4. Method-of-Moments Approach for Truncated Structures

Azimuthally symmetric truncated structures have been further analyzed by extending a previously developed ad-hoc MoM code for the treatment of annular slots in a perfectly conducting plane [39]. The reference structure considered in [39] is a parallel-plate-waveguide (PPW) with thickness h and perfectly conducting (PEC) plates, possibly filled with a stratified dielectric medium, in which a series of N concentric annular slots is etched in the upper plate (the top view of this kind of structure is shown in Fig. 3). The continuity of the tangential magnetic fields across the slots is here replaced by an impedance boundary condition (IBC). Such boundary condition is enforced in the *space domain*, under the simplifying assumption that the surface impedance can be considered *independent* of the radial wavenumber (i.e., it is not spatially dispersive). This is indeed the case for specific classes of metasurfaces, such as those based on concentric annular narrow slots or strips. In other cases, spatial dispersion can be treated approximately by evaluating the surface impedance for a fixed value of the wavenumber, corresponding to that of a suitable average field. This is a reliable approximation when the field excited by the source is dominated by a given leaky-wave or surface-wave field, as occurs in cylindrical LWAs [28] or holographic [45] antennas, respectively. Finally, the present MoM formulation can be used for the analysis of radially non-uniform metasurfaces, whose locally homogenized surface impedance is a step-wise function of the radial coordinate ρ (e.g., the surface impedance can vary between adjacent slots). This feature can be useful for the analysis of radially tapered 2-D LWAs [40].

Assuming for simplicity that no TM/TE coupling occurs, the TM and TE polarizations can be treated separately. In the TM case, the relevant integral equation can be written as

$$-j\omega\epsilon_0 \int_{\text{slots}} g^{\text{TM}}(\rho, \rho') M_\phi(\rho') \rho' d\rho' - Y_S^{\text{TM}}(\rho) M_\phi(\rho) = H_\phi^{\text{in}}(\rho) \quad (19)$$

where $Y_S^{\text{TM}} = 1/Z_S^{\text{TM}}$ is the TM surface admittance and $g^{\text{TM}}(\rho, \rho')$ is the kernel valid for slots (i.e., for the case $Y_S^{\text{TM}} = 0$; its expression is derived in [39]). The MoM matrix elements Y_{ij}^{TM} , resulting from a Galerkin discretization of (19) with subsectional basis functions $\Lambda_j^{\text{TM}}(\rho)$, can then be written as

$$Y_{ij}^{\text{TM}} = Y_{ij}^{\text{TM},0} + \int_{\text{slots}} Y_S^{\text{TM}}(\rho) \Lambda_i^{\text{TM}}(\rho) \Lambda_j^{\text{TM}}(\rho) d\rho \quad (20)$$

Here $Y_{ij}^{\text{TM},0}$ are the corresponding elements valid for the case of slots; these can be evaluated very efficiently in the spectral (Fourier-Bessel) domain by employing suitable basis functions (see [39]). The additional term, which accounts for the nonzero surface admittance of the metasurface, is different from zero only for pairs of basis functions with overlapping support and can easily be evaluated numerically or even analytically.

Similarly, in the TE case, the relevant integral equation can be written as

$$\int_{\text{slots}} g^{\text{TE}}(\rho, \rho') M_\rho(\rho') \rho' d\rho' + Y_S^{\text{TE}}(\rho) M_\rho(\rho) = H_\rho^{\text{in}}(\rho) \quad (21)$$

where $Y_S^{\text{TE}} = 1/Z_S^{\text{TE}}$ is the TE surface admittance and $g^{\text{TE}}(\rho, \rho')$ is the kernel valid for slots (see [39]). The resulting MoM matrix elements are then

$$Y_{ij}^{\text{TE}} = Y_{ij}^{\text{TE},0} + \int_{\text{slots}} Y_S^{\text{TE}}(\rho) \Lambda_i^{\text{TE}}(\rho) \Lambda_j^{\text{TE}}(\rho) d\rho \quad (22)$$

and considerations similar to the TM case can be done about the evaluation of the term that takes into account a finite surface admittance.

3. NUMERICAL RESULTS

The analytical and numerical approaches described in the previous sections have been tested for the reference structure in Fig. 2. The far field excited by both a VED (TM waves) and a VMD (TE waves) has been calculated for various geometries of the metasurface covering the grounded slab, based on concentric annular slots or rings (see Fig. 3) and concentric annular array of patches (see Fig. 4).

The linearized structure corresponding to the geometry in Fig. 3 are linear arrays of metal strips placed at the interface between two possibly different dielectric media. Analytical formulas are available

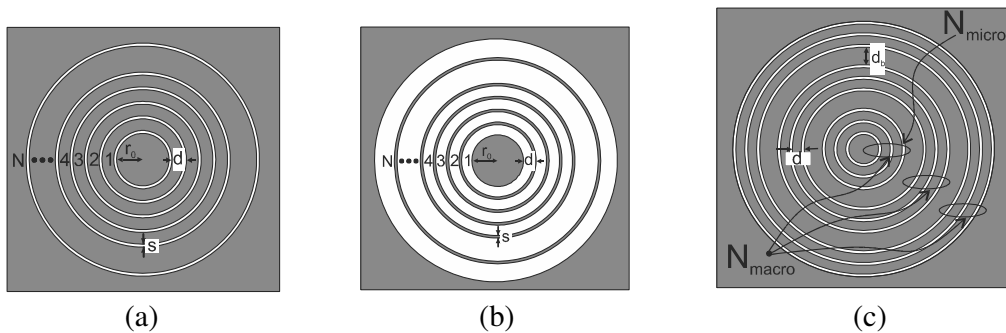


Figure 3. Geometry of the annular metasurfaces based on arrays of slots or rings considered in the numerical simulations. (a) Narrow slots of width s and radial period d . (b) Narrow strips of width s and radial period d . (c) N_{macro} clusters of N_{micro} slots, with radial spacing between adjacent clusters d_b .

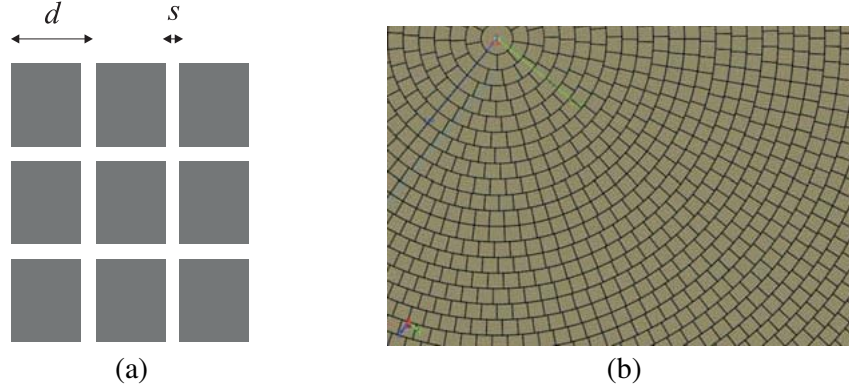


Figure 4. Geometry of the metasurface constituted by radial arrays of annularly disposed patches considered in the numerical simulations. (a) The linearized patch array structure: width of the slots s and period d . (b) Top view of a sector of the truncated radial array of patches.

for the homogenized surface impedance of such linear arrays [35]. Assuming slots of width s and period d etched in a perfectly conducting metal plate and embedded in a uniform medium with wavenumber $k = 2\pi/\lambda$ and characteristic impedance η , for TM fields propagating orthogonally to the strips it results in

$$Z_S^{\text{TM}} = j \frac{\eta kd}{2\pi} \ln \csc \left(\frac{\pi s}{2d} \right) \quad (23)$$

Dually, for TE fields propagating orthogonally along linear arrays of perfectly conducting strips of width s and period d it results in

$$Y_S^{\text{TE}} = j \frac{2kd}{\eta\pi} \ln \csc \left(\frac{\pi s}{2d} \right) \quad (24)$$

Both formulas are accurate for thin slots and strips, respectively, i.e., $s \ll d$, and dense grids, i.e., $d \ll \lambda$; within these limits, the structure is not spatially dispersive. When the media on the two sides of the array are different, the parameters k and η to be used in (23), (24) are those of an effective medium with relative permittivity equal to the average of those of the two media.

In the first set of results the PO approach for the evaluation of the far-field pattern of truncated structures (TEN-PO approach in Section 2.3) has been validated against the far-field of the infinite structure (TEN approach in Section 2.2) by increasing the effective aperture of the truncated structure. In Fig. 5(a) a grounded slab with $\varepsilon_r = 1$ and thickness $h = 14.37$ mm, covered with a metasurface as in Fig. 3(a), has been excited by a VED at the frequency $f = 16$ GHz. The radius r_0 of the internal circular metallic patch and the radial period are both equal to 3 mm; the width of the slots is 0.1 mm. The *solid black* line represents the solution obtained using the TEN model for the calculation of the far-field pattern. The other solutions are those obtained by considering the truncation effects with the PO approach. In particular, the cases shown are those for an effective aperture that is 30, 100, and 500 periods wide. It is clearly visible that, as the effective aperture of the truncated structure becomes larger, the TEN-PO solution converges, as expected, to that based on the TEN that models the infinite metasurface.

The same considerations can be done for the results presented in Fig. 5(b). In this case the structure is excited by a VMD and the geometry of the screen is shown in Fig. 3(b). The structure can be seen as the complementary case respect to the previous one (i.e., now the width of the strips is 0.1 mm). However, we note that the two cases shown in Fig. 5 present different convergence behaviors, since in Fig. 5(a) a good agreement between TEN and TEN-PO approaches is obtained for an effective aperture of 100 periods, whereas 500 periods are needed in Fig. 5(b). This is a consequence of the different decays of the fields excited in the two structures. In fact, in the structure with parameters as in Fig. 5(b) a TE leaky mode with a low attenuation constant is excited, which requires, for the PO approximation to be valid, a higher effective aperture with respect to that needed by the highly attenuated TM field in Fig. 5(a).

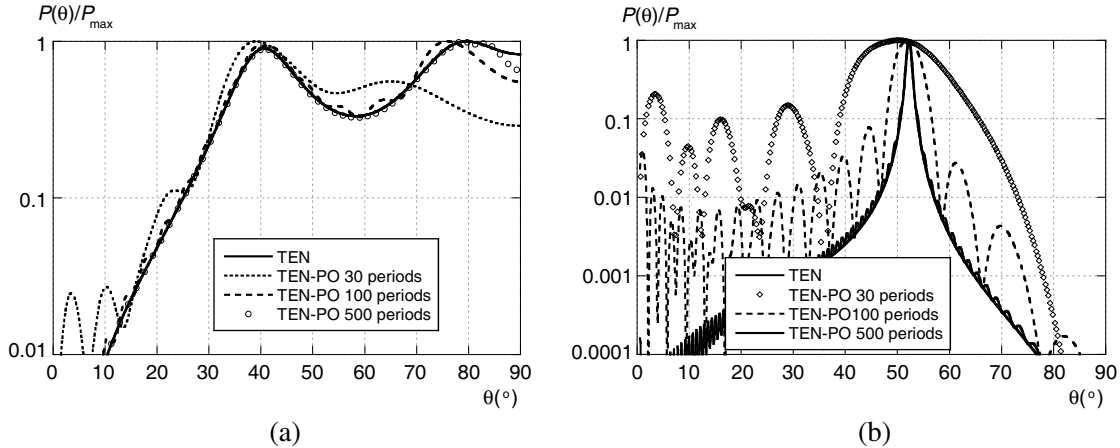


Figure 5. (a) Normalized power radiation patterns for a structure as in Fig. 2(a), with an omnidirectional metasurface as in Fig. 3(a), excited by a VED source placed on the ground plane (TM field): results obtained with the TEN and TEN-PO approaches. *Parameters:* $h = 14.37$ mm, $\epsilon_r = 1$, $f = 16$ GHz, $r_0 = 3$ mm, $d = 3$ mm, $s = 0.1$ mm. (b) Normalized power radiation patterns for a structure as in Fig. 2(a), with an omnidirectional metasurface as in Fig. 3(b), excited by a VMD source placed at $z = -h/2$ (TE field): results obtained with the TEN and TEN-PO approaches. *Parameters:* $h = 14.37$ mm, $\epsilon_r = 1$, $f = 16$ GHz, $r_0 = 3$ mm, $d = 3$ mm, $s = 0.1$ mm.

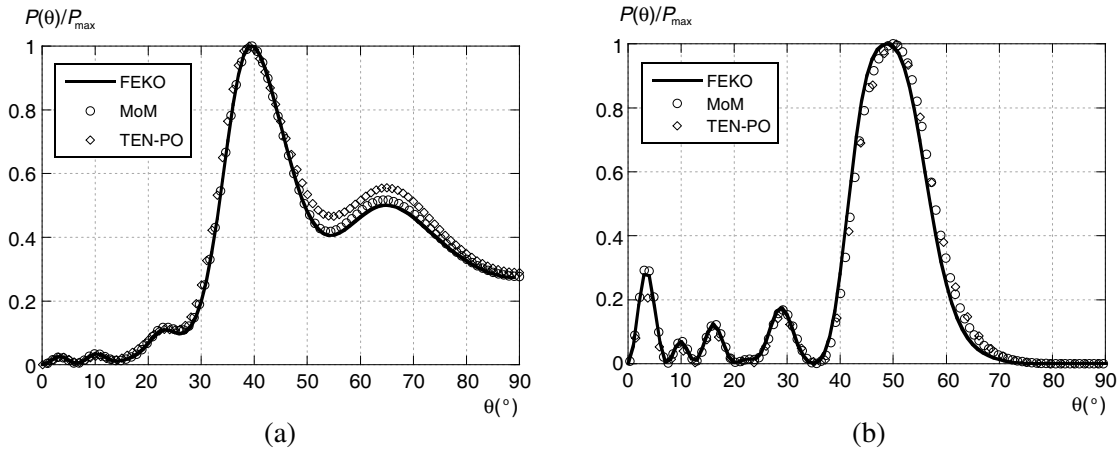


Figure 6. (a) Normalized power radiation patterns for a structure as in Fig. 5(a) (TM field), but with $N = 30$ slots: comparison of the results obtained with the TEN-PO and MoM approaches with those obtained with full-wave simulation software (FEKO). (b) Normalized power radiation patterns for a structure as in Fig. 5(b) (TE field), but with $N = 30$ slots: comparison of the results obtained with the TEN-PO and MoM approaches with those obtained with full-wave simulation software (FEKO).

In the following, the far field of *finite* structures is evaluated with three different numerical and analytical methods: a full-wave EM commercial software (FEKO) [41], the specific MoM formulation presented in Section 2.4 and the TEN-PO approach. As concerns FEKO, the specific numerical tool based on the MoM in the space domain has been used, where apertures on the upper PEC plate of a PPW have been discretized with Rao-Wilton-Glisson basis functions. With this choice, the same background PPW structure has been adopted both in FEKO and in the ad-hoc MoM formulation in Section 2.4. In Fig. 6(a) (TM fields) and in Fig. 6(b) (TE fields), results are presented for finite structures (with $N = 30$ periods) with parameters as in Figs. 5(a) and 5(b), respectively. The results of the MoM, for non-spatially dispersive structures as those in Fig. 3, are in excellent agreement with those obtained with FEKO; those provided by the PO are in good agreement as well, since in this case the

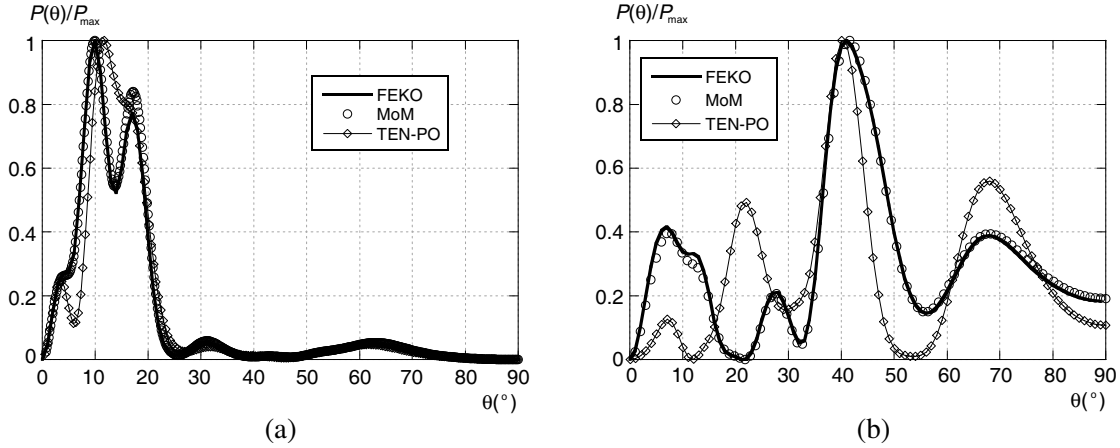


Figure 7. (a) Normalized power radiation patterns for a structure as in Fig. 2(a), with an omnidirectional metasurface as in Fig. 3(b), excited by a VMD source placed at $z = -h/2$ (TE field): comparison of the results obtained with the TEN-PO and MoM approaches with those obtained with full-wave simulation software (FEKO). *Parameters:* as in Fig. 6(b) with $h = 28.37$ mm. (b) Normalized power radiation patterns for a structure as in Fig. 2(a), with an omnidirectional metasurface as in Fig. 3(c), excited by a VED source placed on the ground plane (TM field): comparison of the results obtained with the TEN-PO and MoM approaches with those obtained with full-wave simulation software (FEKO). *Parameters:* as in Fig. 6(a) with $N_{\text{macro}} = 3$, $N_{\text{micro}} = 10$, $d_b = 2d$.

amplitude of the reflected wave at the edges of the effective aperture is sufficiently small with respect to the amplitude of the direct wave.

In Fig. 7(a) and in Fig. 7(b) (TE and TM, respectively), two cases are shown in which the PO approach does not give accurate results. In particular, in both cases we changed slightly the reference structures for Figs. 6(b) and 6(a), respectively. In Fig. 7(a) the same structure of Fig. 6(b) is considered, but with the thickness of the substrate modified from $h = 14.37$ mm to $h = 28.37$ mm. In this case radiation is mainly due to a TE cylindrical leaky wave propagating radially; by increasing the substrate thickness it can be shown that the attenuation constant of the leaky wave is reduced, so that the amplitudes of the incident wave and that of the associated reflected wave at the outer edge are not negligible, resulting in a reduced accuracy of the PO approximation (notably, in the main-beam region). The MoM results are instead in excellent agreement with those obtained with FEKO, since in both cases a PPW background structure is considered that accounts for the same truncation effects.

A different case is illustrated in Fig. 7(b), where we changed the reference structure of Fig. 6(a) by grouping the 30 slots into 3 clusters ($N_{\text{macro}} = 3$) of 10 slots each ($N_{\text{micro}} = 10$), separated by a distance $d_b = 2d$. The geometry of the screen appears as in Fig. 3(c) and represents a very simple case of radially non-uniform metasurface. In this case, while the MoM formulation still gives results in good agreement with the full-wave approach, the PO is much less accurate, since the field on the macro-rings is considerably different from the unperturbed field on an infinite screen due to multiple diffraction at internal edges.

When radially non-uniform metasurfaces are analyzed, e.g., in the case of 2-D LWAs with a radially tapered illumination, the accuracy of the MoM approach proposed here is expected to decrease, since the underlying assumption of local periodicity becomes less valid. A specific investigation has then been carried out on the limits of validity of the homogenized MoM approach as a function of the number of spatial periods N , considering structures with different radial periods at a fixed frequency (hence, with different d/λ ratios).

In Fig. 8 a representative set of results of this kind is shown for a structure as in Fig. 2(a), with an omnidirectional metasurface as in Fig. 3(a), excited by a VED source (TM field). It can be noted that, when d/λ is sufficiently small (of the order of 0.16 or smaller) the homogenized MoM approach produces results in excellent agreement with full-wave (FEKO) results also for very small numbers of slots (down to $N = 2$). On the other hand, by increasing d/λ the accuracy of results

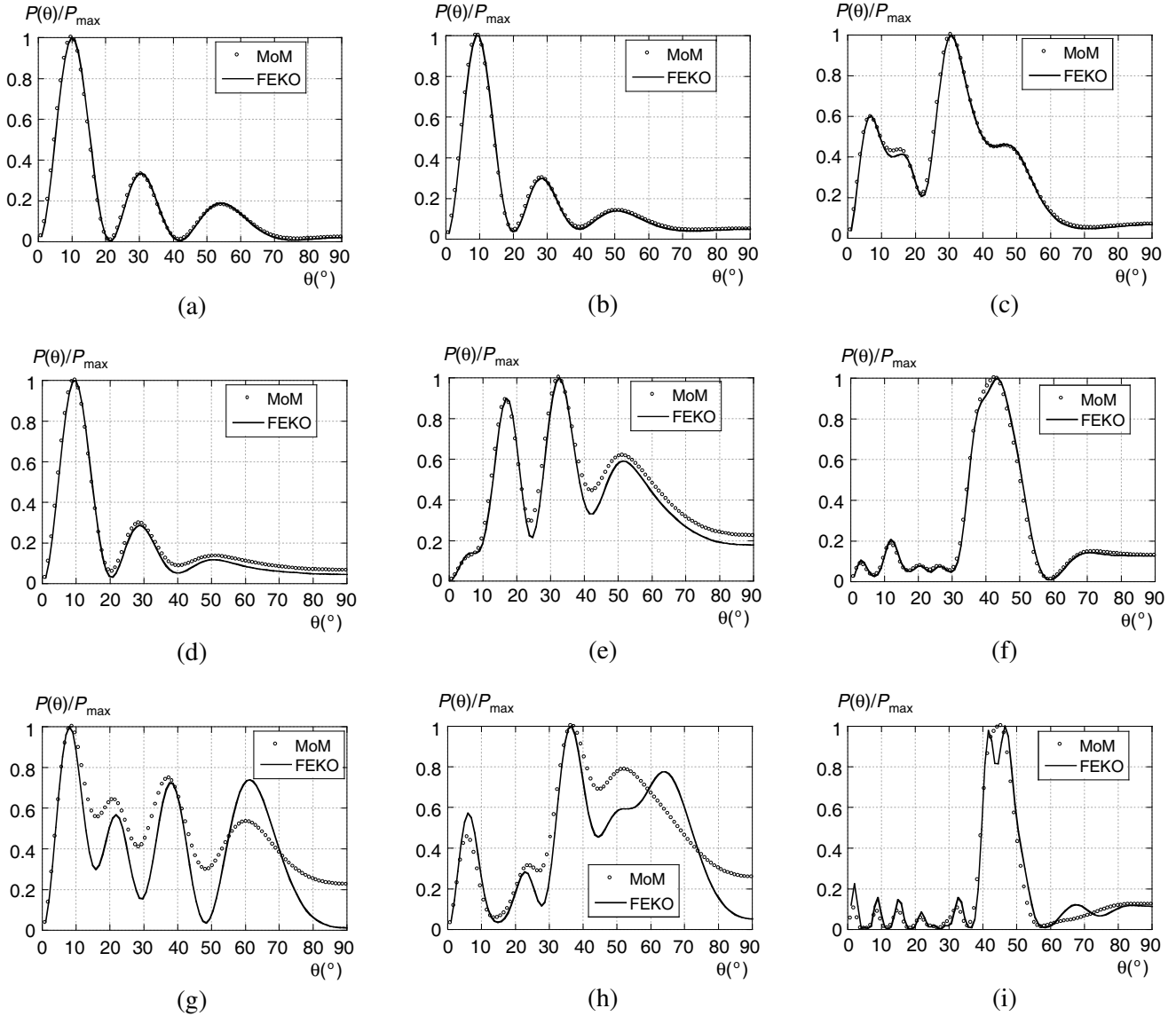


Figure 8. Comparison between MoM and FEKO for a structure as in Fig. 2(a), with an omnidirectional metasurface as in Fig. 3(a), with $h = 14.37$ mm, $\epsilon_r = 1$, $r_0 = 30$ mm, excited at $f = 16$ GHz by a VED placed along the z axis at $z = -h$ (TM polarization), for different radial periods d and different number of slots N . $d = 3$ mm ($d/\lambda = 0.16$): (a) $N = 2$, (b) $N = 4$, (c) $N = 16$; $d = 6$ mm ($d/\lambda = 0.32$): (d) $N = 2$, (e) $N = 4$, (f) $N = 16$; $d = 9$ mm ($d/\lambda = 0.48$): (g) $N = 2$, (h) $N = 4$, (i) $N = 16$.

obtained with small N decreases; in other words, when the spatial period becomes a significant fraction of the wavelength (i.e., the homogenization limits are being approached) a larger number of spatial periods is required to obtain accurate results. This can be related to the edge effects in finite periodic structures. As is known, the homogenized model assumes that: the periodic structure is infinite, a single unit cell is needed to represent the electromagnetic field, and the field is accurately described by the fundamental spatial harmonic (i.e., the higher-order spatial harmonics are negligible) [35,46]. When finite periodic structures are considered, cells at the edges can behave differently from those in the middle of the periodic structures (which should better approximate the unit-cell behavior). The nature of this difference can be strictly related to the contribution of the higher-order spatial harmonics in the representation of the unit-cell field in the infinite periodic structure (i.e., if higher-order spatial harmonics are not negligible, edge effects are more pronounced). Hence, if the homogenization limits

are widely satisfied, higher-order spatial harmonics do not contribute significantly to the representation of the unit-cell field, hence the behavior of the cells at the edges of a truncated structure is similar to that of the relevant unit cell. This justifies the accuracy of the homogenized model observed in Fig. 8 for low values of d/λ and small N .

These considerations provide useful guidelines not only for determining the minimum radial size of uniform homogenized rings but also to assess the minimum length scale for the spatial variation of the homogenized impedance in radially non-uniform structures; in particular, it is expected that a fast radial variation of the homogenized impedance may be accommodated only by operating well within the homogenization limits.

In Fig. 4(a) the linearized structure corresponding to the geometry in Fig. 4(b), i.e., the radial array of annularly disposed square patches, is shown. The radial period of the annular structure is equal to d and the width of the annular slots is s . The number of square patches, with edge length $d - s$ as in Fig. 4(a), is chosen for each ring in order to obtain the azimuthal period which is closest to d . With this choice the omnidirectional annular structure in Fig. 4(b) can be homogenized as the corresponding linearized version, i.e., the 2-D periodic array of square patches in Fig. 4(a). Analytical formulas are available for the homogenized surface impedance of such array [35]. Assuming perfectly conducting patches of edge width $d - s$ and period d , embedded in a uniform medium with wavenumber $k = 2\pi/\lambda$ and characteristic impedance η , for TE fields propagating along the symmetry planes it results in

$$Z_S^{\text{TE}} = -j \frac{\eta}{2 \frac{kd}{\pi} \ln \csc \left(\frac{\pi s}{2d} \right)} \frac{1}{\left(1 - \frac{k_\rho^2}{2k_0^2} \right)} \quad (25)$$

As for the linear array of slots (strips), (25) is accurate for thin slots, i.e., $s \ll d$, and dense grids, i.e., $d \ll \lambda$; furthermore, when the media on the two sides of the array are different, the parameters k and η to be used in (25) are those of an effective medium with relative permittivity equal to the average of those of the two media. We note that the structure described from (25) is spatially dispersive. We remind that spatial dispersion is intrinsically taken into account by the TEN and TEN-PO approaches in Sections 2.2 and 2.3, respectively, whereas can be approximately considered by the MoM method in Section 2.4, assuming that the field excited by the elementary source is dominated by a given surface or leaky wave. In the latter case, the radial propagation wavenumber $k_\rho^{\text{SW/LW}}$ of the relevant surface or leaky wave is used in (25).

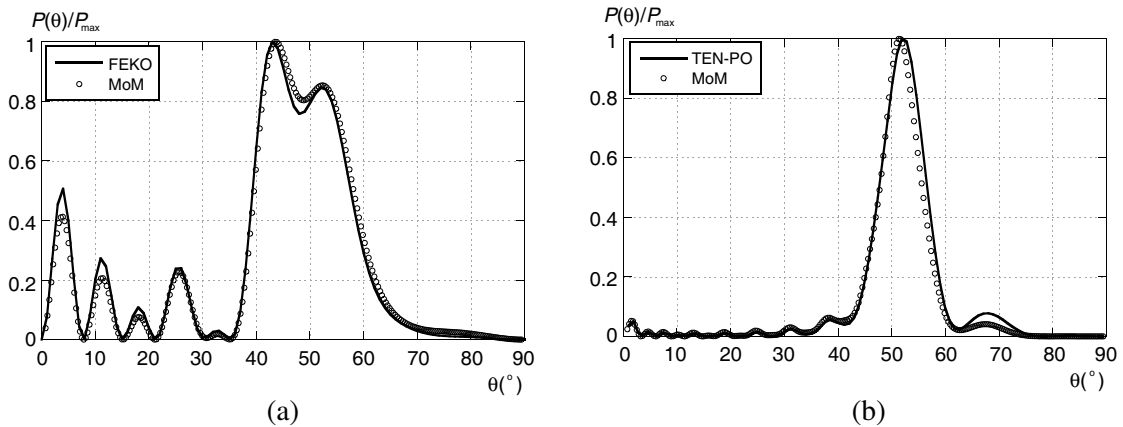


Figure 9. Normalized power radiation patterns for a structure as in Fig. 2(a), with an omnidirectional metasurface as in Fig. 4, excited by a VMD source placed at $z = -h/2$ (TE field). *Parameters:* $h = 15$ mm, $\varepsilon_r = 1$, $f = 18$ GHz, $r_0 = 3$ mm, $d = 2.3$ mm, $s = 0.05$ mm. (a) Comparison of the results obtained with the MoM numerical method with those obtained with full-wave simulation software (FEKO) for an annular structure with total radial length equal to $N = 30$ radial periods. (b) Comparison of the results obtained with the TEN-PO approach with those obtained with the MoM numerical method for an annular structure with total radial length equal to $N = 75$ radial periods.

In Fig. 9, radiation patterns are presented for a LWA based on a concentric annular array of patches as in Fig. 4(b). The VMD source is placed in the middle of the open waveguide and the antenna is designed to excite the fundamental TE_1 leaky mode, i.e., the perturbed TE_1 mode of the equivalent parallel-plate waveguide. The normalized radial propagation wavenumber of the considered leaky mode at 18 GHz is $k_\rho^{LW}/k_0 = \beta_\rho^{LW}/k_0 - j\alpha_\rho^{LW}/k_0 = 0.784 - j0.024$, where k_0 is the free-space wavenumber. A normalized phase constant $\beta_\rho^{LW}/k_0 = 0.784$ corresponds to a main-beam pointing angle of 51° (i.e., $\theta^{LW} \cong \sin(\beta_\rho^{LW}/k_0) \cong 51^\circ$) from broadside, whereas a normalized attenuation constant $\alpha_\rho^{LW}/k_0 = 0.024$ requires an effective aperture of at least $N = 60d$, with radial periods $d = 2.3$ mm, in order the 90% of the power associated to the excited leaky wave to be radiated [27].

In Fig. 9(a) the far field of a finite structures (with $N = 30$ periods) is shown. The result of the MoM, which is approximate for a spatially dispersive structure, is fully validated against that obtained with FEKO; a very good agreement between the two different numerical methods is observed. Results provided by the PO are not shown in Fig. 9(a), since a higher number of radial periods (more than $N = 60$) is needed in order the PO approximation to be valid. The simulation with FEKO took 45 GB of RAM and 15 hours of parallel processing on 10-cores Intel(R) Core(TM)-i7 CPU; unfortunately, it was not possible to further increase the number of radial periods to be simulated. On the other hand, the simulation with the MoM numerical method took less than 15 minutes with a negligible usage of RAM. In Fig. 9(b) the far field of a finite structures with $N = 75$ periods (more than the 90% of the power associated to the excited leaky wave is radiated) is shown. The result of the TEN-PO is in excellent agreement with that obtained with the MoM. The pointing angle of the LWA is close to 51° , as predicted by the theory, and the sidelobe level is sufficiently low. We finally note that in order to obtain the results in Fig. 9(b) the MoM took about 30 MB of RAM and 1 hour of parallel processing, while the TEN-PO method 15 seconds and an insignificant RAM consumption.

4. CONCLUSION

In this paper different homogenization-based approaches have been presented for the analysis of planar omnidirectional structures. An unconventional use of the ordinary impedance boundary condition, in the form of a simple dot product relation between the average tangential electric field and the average tangential electric current, has been adopted to establish a transverse equivalent network for planar structures including thin omnidirectional metasurfaces of infinite extent and thereby obtaining the field radiated by vertical dipole sources in closed form. This approach has been improved, at a minimum computational cost, by implementing a physical-optics technique to model truncation effects from circular boundaries and thus evaluate the field radiated by laterally finite structures.

The exact determination of the truncation effects and the generalization to omnidirectional metasurfaces with radially varying surface impedance generally requires, on the other hand, a numerical approach. This has been based here on a suitable extension of a recently proposed efficient method of moments in the spectral Fourier-Bessel domain, in which the metasurface impedance is allowed to have an arbitrary radial variation, but is assumed to be constant with respect to the radial wavenumber (i.e., spatial dispersion of the surface impedance is neglected or considered under suitable approximations). All the approaches gave consistent results and are in good agreement with those provided through full-wave simulations. Future work will address the problem of rigorously taking into account the spatially dispersive nature of the impedance boundary condition used in the moment-method analysis and the design of practical feeds acting as efficient leaky-wave launchers.

APPENDIX A. FAR-FIELD CALCULATION VIA RECIPROCITY

In this Appendix the azimuthally symmetric far field radiated by a vertical electric dipole (VED) or a vertical magnetic dipole (VMD) placed in a planar stratified environment within the half space $z < 0$ is calculated applying the Reciprocity Theorem. The stratified medium is assumed to include an omnidirectional metasurface modeled through the unconventional spectral impedance dyadic (6). For simplicity, it will be assumed that $Z^{\text{TM}/\text{TE}} = Z^{\text{TE}/\text{TM}} = 0$, i.e., no TM/TE coupling, so that the two polarizations can be treated separately. Since they are dual, only the TM case, corresponding to

excitation with a VED, will be considered explicitly.

Let then $\mathbf{E}^A = E_\theta^A(r, \theta)\theta_0$, $\mathbf{H}^A = H_\phi^A(r, \theta)\theta_0$ be the far field radiated in the half space $z > 0$ by a VED $\mathbf{J}^A = \mathbf{z}_0 P_0 \delta(\rho)\delta(z - z_0)/(2\pi\rho)$ placed along the z axis at $z = z_0$, with $[P_0] = [A \cdot m]$, and let us consider as a test source the magnetic ring $\mathbf{M}^B = \phi_0 Q_0 \delta(\rho - \rho')\delta(z - z')/(2\pi\rho)$, with $\rho' = r \sin \theta$, $z' = r \cos \theta$ and $[Q_0] = [V \cdot m]$ (see Fig. A1). The Reciprocity Theorem applied to the whole space reads

$$- \int \mathbf{M}^B \cdot \mathbf{H}^A d\tau = \int \mathbf{J}^A \cdot \mathbf{E}^B d\tau \quad (\text{A1})$$

For the given sources this becomes

$$-2\pi Q_0 H_\phi^A(r, \theta) = P_0 E_z^B(\rho = 0, z = z_0) \quad (\text{A2})$$

hence the calculation of $H_\phi^A(r, \theta)$ is reduced to that of $E_z^B(\rho = 0, z = z_0)$. The latter can in turn be expressed in terms of the magnetic field $\mathbf{H}^B = H_\phi^B(\rho, z)\phi_0$ using Maxwell equations:

$$E_z^B(\rho, z) = \frac{1}{j\omega\varepsilon} \frac{1}{\rho} \frac{\partial}{\partial \rho} (\rho H_\phi^B) \quad (\text{A3})$$

where $\varepsilon = \varepsilon_0 \varepsilon_r$ is the permittivity at $z = z_0$.

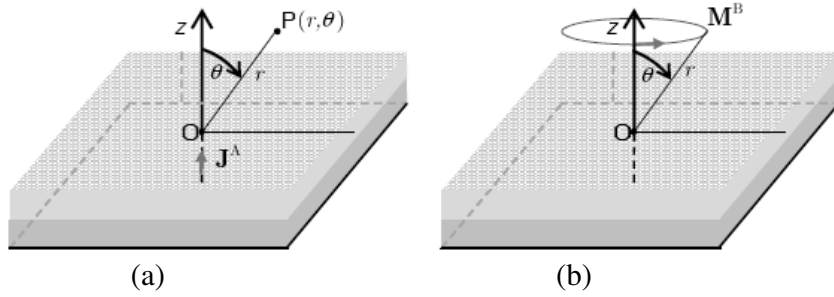


Figure A1. Application of Reciprocity Theorem for the calculation of the far field radiated by a VED (or a VMD) in the presence of a dielectric multilayer including an homogenized omnidirectional metasurface. (a) Original problem; (b) auxiliary problem with a magnetic (or electric) ring source.

The magnetic field $H_\phi^{B,in}(\rho, z)$ produced by the B source in free space and incident on the stratified structure can be expressed as an inverse Fourier-Bessel transform of order 1 [47]:

$$H_\phi^{B,in}(\rho, z) = -j\omega\varepsilon_0 Q_0 \int_0^{+\infty} \frac{e^{jk_z(z-z')}}{2jk_z} J_1(k_\rho \rho') J_1(k_\rho \rho) k_\rho dk_\rho \quad (\text{A4})$$

Since we are interested in calculating the A field in the far region, an asymptotic evaluation of (A4) is performed in the limit $k_0 r \gg 1$; a standard application of the saddle-point technique gives

$$H_\phi^{B,in}(\rho, z) \sim \frac{k_0 Q_0}{2\eta_0} \frac{e^{-jk_0 r}}{r} e^{j\bar{k}_z z} J_1(\bar{k}_\rho \rho) \quad (\text{A5})$$

where $\bar{k}_z = k_0 \cos \theta$ and $\bar{k}_\rho = k_0 \sin \theta$. The incident magnetic field (A5) can then be cast in the form

$$H_\phi^{B,in}(\rho, z) = I^{\text{TM},in}(z) h_\phi(\rho) \quad (\text{A6})$$

where

$$\begin{aligned} I^{\text{TM},in}(z) &= I_0^{\text{TM},in} e^{j\bar{k}_z z} \\ I_0^{\text{TM},in} &= \frac{k_0 Q_0}{2\eta_0} \frac{e^{-jk_0 r}}{r} \\ h_\phi(\rho) &= J_1(\bar{k}_\rho \rho) \end{aligned} \quad (\text{A7})$$

The current $I^{\text{TM}}(z_0)$ is proportional to $I^{\text{TM},in}(0) = I_0^{\text{TM},in}$ times a constant $C = C(\theta)$ that depends on the specific stratified medium and can easily be calculated from the relevant equivalent transmission-line model. Hence the magnetic field at $z = z_0$ is

$$H_\phi^B(\rho, z) = I^{\text{TM}}(z_0)h_\phi(\rho) = C(\theta)I_0^{\text{TM},in}h_\phi(\rho) \quad (\text{A8})$$

From (A3), (A8) we have

$$E_z^B(\rho, z_0) = \frac{1}{j\omega\varepsilon} \frac{1}{\rho} \frac{\partial}{\partial \rho} [\rho h_\phi(\rho)] C(\theta) I_0^{\text{TM},in} \quad (\text{A9})$$

Taking into account (A7) and using standard relations between Bessel functions and their derivatives one has

$$E_z^B(\rho, z_0) = \frac{1}{j\omega\varepsilon} \bar{k}_\rho J_0(\bar{k}_\rho \rho) C(\theta) I_0^{\text{TM},in} \quad (\text{A10})$$

hence

$$E_z^B(0, z_0) = \frac{1}{j\omega\varepsilon} \bar{k}_\rho C(\theta) I_0^{\text{TM},in} \quad (\text{A11})$$

Finally, from (A2), (A7), and (A11)

$$H_\phi^A(r, \theta) = -\frac{P_0}{2\pi Q_0} \frac{1}{j\omega\varepsilon} \bar{k}_\rho C(\theta) I_0^{\text{TM},in} = \frac{P_0}{\varepsilon_r} jk_0 \sin \theta C(\theta) \frac{e^{-jk_0 r}}{4\pi r} \quad (\text{A12})$$

so that, taking into account that in the far region $E_\theta = \eta_0 H_\phi$, (10) is proved.

It is interesting to note that the same result would be obtained using the standard reciprocity-based approach that uses a point dipole in the far region as a test source. This can be justified taking into account again that the plane-wave spectrum of the asymptotic field (A5) produced by the magnetic ring source is azimuthally symmetric and comprised of plane waves having the same wavenumber k_z , each corresponding to the far field radiated by the elementary dipoles in which the ring source can be decomposed; furthermore, all of these plane waves have the same interaction with the stratified medium, in view of the assumed form (6) for the homogenized impedance of the metasurface. Therefore, all the elementary dipoles in which the ring source can be decomposed give the same contribution to the field E_z^B .

REFERENCES

1. Baccarelli, P., P. Burghignoli, G. Lovat, and S. Paulotto, "A novel printed leaky-wave 'bull-eye' antenna with suppressed surface-wave excitation," *Digest 2004 IEEE AP-S Symp. Ant. Prop.*, Vol. 1, 1078–1081, 2004.
2. Llombart, N., A. Neto, G. Gerini, and P. de Maagt, "Planar circularly symmetric EBG structures for reducing surface waves in printed antennas," *IEEE Trans. Antennas Propag.*, Vol. 53, No. 10, 3210–3218, Oct. 2005.
3. Sutinjo, A., M. Okoniewski, and R. H. Johnston, "A holographic antenna approach for surface wave control in microstrip antenna applications," *IEEE Trans. Antennas Propag.*, Vol. 58, No. 3, 675–682, Mar. 2010.
4. Podilchak, S. K., Y. M. M. Antar, A. P. Freundorfer, P. Baccarelli, P. Burghignoli, S. Paulotto, and G. Lovat, "Planar antenna for continuous beam scanning and broadside radiation by selective surface wave suppression," *Electronics Letters*, Vol. 46, No. 9, 613–614, Apr. 2010.
5. Houaneb, Z., H. Zairi, A. Gharsallah, and H. Baudrand, "Analysis of a new annular multi-slits antenna using wave concept iterative process in cylindrical coordinates," *Ann. Telecommun.*, Vol. 66, 383–394, 2011.
6. Podilchak, S. K., P. Baccarelli, P. Burghignoli, A. P. Freundorfer, and Y. M. M. Antar, "Optimization of a planar bull-eye leaky-wave antenna fed by a printed surface-wave source," *IEEE Antennas Wireless Propag. Lett.*, Vol. 12, 665–669, 2013.
7. Ettorre, M. and A. Grbic, "Generation of propagating Bessel beams using leaky modes," *IEEE Trans. Antennas Propag.*, Vol. 60, No. 8, 3605–3613, Aug. 2012.

8. Podilchak, S. K., P. Baccarelli, P. Burghignoli, A. P. Freundorfer, and Y. M. M. Antar, "Analysis and design of annular microstrip-based planar periodic leaky-wave antennas," *IEEE Trans. Antennas Propag.*, Vol. 62, No. 6, 2978–2991, Jun. 2014.
9. Lezec, H. J., A. Degiron, E. Devaux, R. A. Linke, L. Martin-Moreno, F. J. Garcia-Vidal, and T. W. Ebbesen, "Beaming light from a subwavelength aperture," *Science*, Vol. 297, 820–822, Aug. 2002.
10. Jackson, D. R., A. A. Oliner, Y. Zhao, and J. T. Williams, "The beaming of light at broadside through a subwavelength hole: Leaky-wave model and open stopband effect," *Radio Sci.*, Vol. 40, 1–12, 2005.
11. Schuller, J. A., E. S. Barnard, W. Cai, Y. C. Jun, J. S. White, and M. L. Brongersma, "Plasmonics for extreme light concentration and manipulation," *Nature Materials*, Vol. 9, 193–204, Mar. 2010.
12. Fu, Y. and X. Zhou, "Plasmonic lenses: A review," *Plasmonics*, Vol. 5, No. 3, 287–310, Jun. 2010.
13. Bao, Q. and K. Loh, "Graphene photonics, plasmonics, and broadband optoelectronic devices," *ACS Nano*, Vol. 6, No. 5, 3677–3694, 2012.
14. Politano, A. and G. Chiarello, "Plasmon modes in graphene: Status and prospect," *Nanoscale*, Vol. 6, 10927–10940, 2014.
15. Sun, Z., T. Hasan, F. Torrisi, D. Popa, G. Privitera, F. Wang, F. Bonaccorso, D. M. Basko, and A. C. Ferrari, "Graphene mode-locked ultrafast laser," *ACS Nano*, Vol. 4, No. 2, 803–810, 2010.
16. Bonaccorso, F., Z. Sun, T. Hasan, and A. C. Ferrari, "Graphene photonics and optoelectronics," *Nat. Photonics*, Vol. 4, No. 9, 611–622, 2010.
17. Berry, C. W., N. Wang, M. R. Hashemi, M. Unlu, and M. Jarrahi, "Significant performance enhancement in photoconductive terahertz optoelectronics by incorporating plasmonic contact electrodes," *Nat. Commun.*, Vol. 4, 1622, 2013.
18. Politano, A., "Low-energy collective electronic mode at a noble metal interface," *Plasmonics*, Vol. 8, No. 2, 357–360, 2013.
19. Baccarelli, P., P. Burghignoli, D. Comite, D. Di Ruscio, A. Galli, P. Lampariello, and D. R. Jackson, "Annular reconfigurable metasurface for omnidirectional dual-pol leaky-wave antennas," *7th Europ. Conf. Antennas Prop. (EuCAP)*, Gothenburg, Sweden, Apr. 8–11, 2013.
20. Guo, Y. J., A. Paez, R. A. Sadeghzadeh, and S. K. Barton, "A circular patch antenna for radio LANs," *IEEE Trans. Antennas Propag.*, Vol. 45, No. 1, 177–178, Jan. 1997.
21. McEwan, N. J., R. A. Abd-Alhameed, E. M. Ibrahim, P. S. Excell, and J. G. Gardiner, "A new design of horizontally polarized and dual-polarized uniplanar conical beam antennas for HIPERLAN," *IEEE Trans. Antennas Propag.*, Vol. 51, No. 2, 229–237, Feb. 2003.
22. Brégains, J. C., G. Franceschetti, A. G. Roederer, and F. Ares, "New toroidal beam antennas for WLAN communications," *IEEE Trans. Antennas Propag.*, Vol. 55, 389–398, Feb. 2007.
23. Zhou, D., R. A. Abd-Alhameed, C. H. See, N. J. McEwan, and P. S. Excell, "New circularly-polarized conical-beam microstrip patch antenna array for short-range communication systems," *Microw. Opt. Technol. Lett.*, Vol. 51, 78–81, Jan. 2009.
24. Batchelor, J. C. and R. J. Langley, "Microstrip ring antennas operating at higher order modes for mobile communications," *IEE Proc. Microw. Antennas Propag.*, Vol. 142, No. 2, 151–155, Apr. 1995.
25. Ares, F., G. Franceschetti, J. Mosig, S. Vaccaro, J. Vassallo, and E. Noreno, "Satellite communication with moving vehicles on Earth: Two prototype circular array antennas," *Microw. Opt. Technol. Lett.*, Vol. 39, No. 1, 14–16, Oct. 2003.
26. Son, S. H., S. I. Jeon, C. J. Kim, and W. B. Hwang, "GA-based design of multi-ring arrays with omnidirectional conical beam pattern," *IEEE Trans. Antennas Propag.*, Vol. 58, No. 5, 1527–1534, May 2010.
27. Jackson, D. R. and A. A. Oliner, "Leaky-wave antennas," C. A. Balanis (Ed.), *Modern Antenna Handbook*, Ch. 7, Wiley, New York, 2008.
28. Jackson, D. R. and N. G. Alexopoulos, "Gain enhancement methods for printed circuit antennas," *IEEE Trans. Antennas Propag.*, Vol. 33, No. 9, 976–987, Sep. 1985.

29. Feresidis, A. P. and J. C. Vardaxoglou, "High gain planar antenna using optimised partially reflective surfaces," *IEE Proc. Microw. Antennas Propag.*, Vol. 148, No. 6, 345–350, Dec. 2001.
30. Zhao, T., D. R. Jackson, J. T. Williams, H.-Y. D. Yang, and A. A. Oliner, "2-D periodic leaky-wave antennas — Part I: Metal patch design; Part II: Slot design," *IEEE Trans. Antennas Propag.*, Vol. 53, No. 11, 3505–3524, Nov. 2005.
31. Costa, F. and A. Monorchio, "Design of subwavelength tunable and steerable Fabry-Perot/leaky wave antennas," *Progress In Electromagnetics Research*, Vol. 111, 467–481, 2011.
32. Sievenpiper, D., "Forward and backward leaky-wave radiation with large effective aperture from an electronically tunable textured surface," *IEEE Trans. Antennas Propag.*, Vol. 53, No. 1, 236–247, Jun. 2005.
33. Patel, A. M. and A. Grbic, "A printed leaky-wave antenna based on a sinusoidally-modulated reactance surface," *IEEE Trans. Antennas Propag.*, Vol. 59, No. 6, 2087–2096, Jun. 2011.
34. Minatti, G., F. Caminita, M. Casaletti, and S. Maci, "Spiral leaky-wave antennas based on modulated surface impedance," *IEEE Trans. Antennas Propag.*, Vol. 59, No. 12, 4436–4444, Dec. 2011.
35. Tretyakov, S., *Analytical Modeling in Applied Electromagnetics*, Sec. 4.4.2, Artech House, Norwood, MA, 2003.
36. Luukkonen, O., C. R. Simovski, G. Granet, G. Goussetis, D. Lioubtchenko, A. Räsänen, and S. A. Tretyakov, "Simple and accurate analytical model of planar grids and high-impedance surfaces comprising metal strips or patches," *IEEE Trans. Antennas Propag.*, Vol. 56, No. 6, 1624–1632, Jun. 2008.
37. Holloway, C. L., E. F. Kuester, J. A. Gordon, J. O'Hara, J. Booth, and D. R. Smith, "An overview of the theory and applications of metasurfaces: The two-dimensional equivalents of metamaterials," *IEEE Trans. Antennas Propag. Mag.*, Vol. 54, No. 2, 10–35, Apr. 2012.
38. Salem, M. A., K. Achouri, and C. Caloz, "Metasurface synthesis for time-harmonic waves: Exact spectral and spatial methods," *Progress In Electromagnetics Research*, Vol. 149, 205–216, 2014.
39. Di Ruscio, D., P. Burghignoli, P. Baccarelli, D. Comite, and A. Galli, "Spectral method of moments for planar structures with azimuthal symmetry," *IEEE Trans. Antennas Propag.*, Vol. 62, No. 4, 2317–2322, Apr. 2014.
40. Gómez-Tornero, J. L., D. Blanco, E. Rajo-Iglesias, and N. Llombart, "Holographic surface leaky-wave lenses with circularly-polarized focused near-fields — Part I: Concept, design and analysis theory," *IEEE Trans. Antennas Propag.*, Vol. 61, No. 7, 3475–3485, Jul. 2013.
41. FEKO Suite 6.0, EM Software and Systems, Technopark, Stellenbosh, 7600, South Africa, 2010; <http://www.feko.co.za>.
42. Rao, S. M., D. R. Wilton, and A. W. Glisson, "Electromagnetic scattering by surfaces of arbitrary shape," *IEEE Trans. Antennas Propag.*, Vol. 30, 409–418, 1982.
43. Felsen, L. and N. Marcuvitz, *Radiation and Scattering of Waves*, Ch. 2, Prentice-Hall, Englewood Cliffs, NJ, 1973.
44. Ostner, H., E. Schmidhammer, J. Detlefsen, and D. R. Jackson, "Radiation from dielectric leaky-wave antennas with circular and rectangular apertures," *Electromagn.*, Vol. 17, No. 5, 505–535, 1997.
45. Fong, B. H., J. S. Colburn, J. J. Ottusch, J. L. Vischer, and D. F. Sievenpiper, "Scalar and tensor holographic artificial impedance surfaces," *IEEE Trans. Antennas Propag.*, Vol. 58, No. 10, 3212–3221, Oct. 2010.
46. Paulotto, S., P. Baccarelli, P. Burghignoli, G. Lovat, G. Hanson, and A. B. Yakovlev, "Homogenized Green's functions for an aperiodic line source over planar densely periodic artificial impedance surfaces," *IEEE Trans. Microwave Theory Tech.*, Vol. 58, No. 7, 1807–1817, Jul. 2010.
47. Dudley, D. G., *Mathematical Foundations for Electromagnetic Theory*, Wiley-IEEE Press, New York, 1994.